Nanoscale

Accepted Manuscript

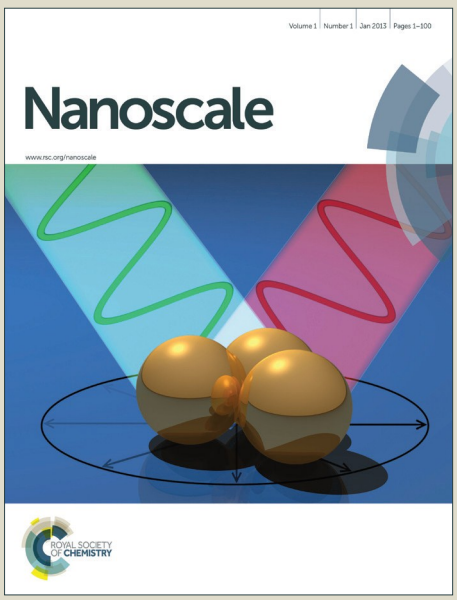

ROYAL SOCIETY OF CHEMISTRY

www.rsc.org/nanoscale

Silica Core - Polystyrene Shell Nanoparticles Synthesis and Assembly in Three Dimensions

Hadi Sabouri [a], Yun Huang [b], Kohji Ohno,[b*] Sébastien Perrier [c,d*]

[a] *Key Centre for Polymers & Colloids, School of Chemistry, The University of Sydney, NSW, Australia*

[b] *Institute for Chemical Research, Kyoto University, Uji, Kyoto 611-0011, Japan.*

[c] *Department of Chemistry, The University of Warwick, Gibbet Hill, Coventry, CV4 7AL, United Kingdom*

[d] *Faculty of Pharmacy and Pharmaceutical Sciences, Monash University, 381 Royal Parade, Parkville, VIC 3052, Australia*

[*] *email: s.perrier@warwick.ac.uk; Tel: +44 (0)2476 528085; Fax: +44 (0)2476 524112*

[*] *email: ohno@scl.kyoto-u.ac.jp; Tel: 0774-38-3163; Fax: 0774-38-3170*

Abstract

Monodisperse silica nanoparticles (SiNP) grafted with well-defined and highly dense polystyrene brushes are used as building blocks for the formation of three-dimensional (3D) colloidal crystals. By adjusting the refractive indices and the density of the hybrid particles with those of mixed solvents, iridescent microcrystals were formed throughout the entire suspension which were characterised by confocal laser microscopy. These core-shell hybrid particles are not charged and the driving force of the crystallization relies on repulsive forces between the polymer brushes with high grafting density. The interparticle distance is correlated to Bragg's Law and can be controlled by manipulating the grafting density and the length of the polymer brushes. Finally, the uniformity of these unique core-shell particles was exploited to generate 3D assemblies by a rapid and simple process based on centrifugation

Introduction

The ability of three-dimensional (3D) periodic dielectric materials to possess a photonic bandgap was first demonstrated by Yablonovitch and John in 1987.[1, 2] As an example of such materials, colloidal crystals (CCs) have attracted increasing attention for their potential applications as photonic crystals[3-6] as well as fundamental studies for condensed matter crystallization,[7-9] waveguides,[10-13] sensors,[14, 15] lasers[16-19] and photonic bandgap materials (PBG).[20-23] These CCs have domains of high and low refractive index with the periodicity on the order of wavelength of visible light. As a result, the CCs have the ability to manipulate the light by the formation of stop bands, in which the propagation of light is forbidden in particular range of wavelengths and directions.[20, 24, 25] Colloidal particles can be formed by hard[26] or soft[27] particles suspended in a liquid. When particles volume fraction reaches a critical point,[28] crystallization happens and colloidal particles arrange themselves in well-defined periodic arrays either in two or three dimensions. This phenomenon, which is called self-assembly, is known as the most feasible route to form CCs. Driven force for the formation of these CCs are mainly hard-sphere[26, 29] (excluded volume repulsions) which is effective in short range and electrostatic potentials[30-32] which can be long range depending on the ionic strength of suspension. A large number of attempts have been made to fabricate 3D colloidal crystals.[27, 33-35] Despite improvements in the process of self-assembly, fabricated CCs typically suffer from a large number of defects.[36-44]

A suspension of spherical silica nanoparticles grafted with concentrated polymer brushes, first observed by Ohno et al.,[34, 45] has advantages over hard and soft colloidal particles in terms of size manipulation and interparticle distancing. In their pioneering work, Ohno et al. showed that colloidal crystals could be obtained from hybrid particles with a shell of well-defined poly(methyl methacrylate) chains densely grafted on the surface of silica cores by atom transfer radical polymerization, and suspended in a good solvent.[33, 46] The same group recently showed that the resulting colloidal crystals can be further immobilized via inter-particle crosslinking of the polymer shell, and still retain their periodically ordered structure.[47] Silica nanoparticles (SiNP) as cores for hybrid particles are a versatile substrate due to their inertness, facile fabrication routes and the feasibility of post-modification of these particles through simple chemical methodologies.[48]

In this study, we used silica nanoparticles with average diameters of 75 and 135 nm to form core-shell hybrid spheres. The hybrid colloidal particles were prepared by reversible addition fragmentation chain transfer (RAFT) polymerisation from the surface of silica nanoparticles (SiNP), in order to generate polymer-shell silica-core nanoparticles.[48-51] RAFT polymerization is one of the most versatile processes, in terms of tolerance towards a wide range of monomer functionality and also high degree of control over the size and uniformity of the polymer chains.[49, 52] Silica particles functionalised with a chain transfer agent (CTA) bearing triethoxysilane moieties (EHT) were used to mediate RAFT polymerisation of styrene.[53] The hybrid particles thus fabricated had highly concentrated polystyrene brushes with different chain lengths and consequently different hydrodynamic diameters. Since these particles are not electrostatically charged, the main interactions between colloidal particles are steric repulsions. In our previous work, we demonstrated the self-assembly into two-dimentional ordered arrays of hybrid particles based on a poly(methyl methacrylate) shell and a silica core.[54] In this work, we investigate the ability of core-shell particles with a polystyrene shell to assemble in three-dimensional lattices, and explore the use of two distinct processes, suspension and centrifugation of the particles. We establish optimal conditions for the use of RAFT polymerisation to obtain high density polystyrene brushes using a free radical initiator rather than styrene auto-initiation. In addition, we show that the narrow size distribution of the particles enables the formation of 3D colloidal crystals with variable reflected colours by simple centrifugation of the colloidal solution, an approach much more versatile, simpler and faster than the sedimentation technique used in previous work.

Experimental Section

Materials

All chemicals were purchased from Sigma Aldrich at highest purity available, unless otherwise stated. Chlorobenzene, *o*-dichlorobenzene, 1,2-dimethoxyethane (DME, 99 %), hydrofluoric acid (HF, 50%), Aliquot 336 (Trioctylmethylammonium chloride) and 1,1'-azobis(cyclohexanecarbonitrile) (V40, 98 %) were used as received. 2,2′-Azobis(isobutyronitrile) (AIBN) was recrystallised twice from

methanol prior to use. Dichloromethane (DCM, AJAX Finechem, 99 %, dehydrated), tetrahydrofuran (THF, AJAX Finechem, 99 %), 1,4-dioxane (MERCK, 99 %) toluene (AJAX Finechem, 99 %), dimethyl formamide (DMF, AJAX Finechem, 99 %), chloroform (Thermo Fisher, 99 %) and ethanol (Redox Chemicals, 99.9 %) were used without further purification. 2-(((Butylthio)carbonothiolyl)thio)propanoic acid (called (propanoic acid)yl butyl trithiocarbonate (PABTC) in this paper was provided by Dr. Algi Serelis from Dulux Group. Silica nanoparticles with average diameter of 135 nm were kindly donated by Nippon Shokubai Co., Ltd., Osaka, Japan. Water was purified by a MilliQ system to a specific resistivity of ~ 18 MΩ·cm. Styrene (S) was purified by flash chromatography over activated neutral alumina before use. All reactions were carried out under a N_2 atmosphere unless otherwise stated.

Characterization

^{1}H-Nuclear Magnetic Resonance (^{1}H NMR). ^{1}H NMR spectra were acquired on a Bruker Avance 200 or 300 MHz at 300K. Deuterated chloroform ($CDCl_3$) was used as solvent. All chemical shifts are reported in ppm (δ).

Dynamic Light Scattering (DLS). Particles size measurements were carried out by DLS using a Malvern Instrument Zetasizer Nano series instrument with a detection angle of 173°, where the intensity-weighted mean hydrodynamic size and the width of the particle size distribution were obtained from CONTIN analysis. Each measurement was repeated three times at 25 °C with an equilibrium time of 2 min before starting measurement. All samples were prepared freshly in ethanol (for bare SiNP) and THF (for SiNP-Polymer) to avoid aggregation. Polydispersity values (*PDI*) were obtained from cumulants measurements.

Size Exclusion Chromatography (SEC). Number-average molar mass ($M_{n,SEC}$) and dispersity ($Đ$) values of the synthesized polymers were measured using SEC on a Shimadzu CBM-20A liquid chromatography system with a Polymer Laboratories Pl-Gel 5 μM guard column and two Polymer Laboratories Pl-Gel Mixed-B columns using THF as the eluent at a flow rate of 1.0 mL·min^{-1} at 40 °C. The system was equipped with a Shimadzu RID-10A differential refractive index detector, Wyatt MiniDawn TREOS light scattering and Wyatt Viscostar-II viscometer. Before the injection (100 μL), the samples were filtered through a polytetrafluoroethylene

(PTFE) membrane with 0.45 μm pores. Narrow polystyrene (PS) standards ($Đ < 1.1$) were used to calibrate the SEC system. Analyte samples contained 0.5 vol % toluene as the flow rate marker.

Thermogravimetric Analysis (TGA). The amount of grafted polymer was investigated using a PerkinElmer Pyris 1 TGA with an average ramp up rate of 20 °C min^{-1}. All the samples were heated to 105 °C and equilibrated at that temperature to remove residual solvent prior to the analysis, then ramped up (20 °C·min^{-1}) to 750 °C under a nitrogen atmosphere (20 mL·min^{-1}). The Pyris Manager software was used to calculate the mass loss.

Transmission Electron Microscopy (TEM). TEM images were acquired using Philips CM120 Biofilter (120 kV) electron microscope with a LaB_6 filament running Gatan Digital Micrograph software. TEM samples were prepared by deposition of a drop of dilute sample (0.3-0.5 wt. %) onto a carbon coated copper grid mesh 200 and dried at ambient temperature.

Differential Scanning Calorimetry (DSC). DSC was carried out using a METTLER TOLEDO (DSC 823e) modulated DSC calibrated using an indium metal standard under a nitrogen atmosphere (60 mL·min^{-1}). For measuring the glass transition temperature (T_g), samples (5-10 mg) were heated in an aluminium pan from room temperature to 150 °C, then cooled to -10 °C, and reheated to 120 °C. This cycle was repeated 3 times. The heating and cooling rate was set to 10 °C·min^{-1}. An empty aluminium pan was used as reference. The T_g value was determined as the midpoint value between the onset and the end of a step transition using the TA Instruments Universal Analysis 2000 software.

Ultraviolet–Visible–Near infrared (UV–Vis–NIR) Spectroscopy. UV–Vis–NIR spectra were recorded on a Cary 5000 spectrophotometer (Agilent Technologies) in transmission and reflection modes. Thin 2 mm quartz cuvette was used in transmission mode. For the solid state spectroscopy of colloidal film in the reflection mode silicon wafer was used as a substrate.

Confocal Laser Scanning Microscope (CLSM).

Confocal laser scanning microscopic (CLSM) observations were made on an inverted type CLSM (LSM 5 PASCAL, Carl Zeiss, Germany) with a 488 nm wavelength Ar laser and ×63 objective (Plan Apochromat, Carl Zeiss) in reflection mode.

Centrifugation. Three centrifuges were used to purify the silica and hybrid particles after preparation. For the large volume of samples, an Allegra X-30 (Beckman Coulter) with 30 ml tubes and a Kubota 7780 (Kubota Corporation) with 250 ml tubes were used. For the small volumes a MiniSpin Plus (Crown Scientific) with 2 ml eppendorf tubes was used.

Optical photographs of colloidal crystals were taken by Canon Sx100 digital camera.

Synthesis of 75 nm silica nanoparticles (SiNP)

In a modification to the method described by Rao et al.,[55] 0.11 mol of water was mixed with 40 ml of absolute ethanol in a round bottom flask which was equipped with a magnetic stirrer bar and then was sonicated for 5 min. 9 mmol of TEOS was then added to reaction mixture. The reaction mixture was stirred at 33 °C for 10 min. To this solution was added 25 mmol of 28 % ammonium hydroxide solution. Stirring continued for 17 hours at the same temperature. A sample was taken after three hours for analysis, at which point the suspension looked slightly turbid.

Attachment of RAFT agent to the surface of silica nanoparticles

A RAFT agent bearing triethoxysilane moieties, 6-(triethoxysilyl)hexyl 2-(((methylthio)carbonothioyl)thio)-2-phenylacetate (EHT) was synthesized as reported previously[53] (Scheme S1, Supporting Information). Synthetic silica nanoparticles (SiNP) were purified from excess ammonium hydroxide by 5 centrifugation and redispersion cycles in absolute ethanol. In the case of the suspension of commercially supplied silica nanoparticle in ethylene glycol, the solvent was exchanged to ethanol by dilution of the sample with ethanol followed by centrifugation. The supernatant solution was discarded and the sedimented SiNP were redispersed in ethanol followed by centrifugation. This cycle was repeated three times to obtain a SiNP suspension in ethanol. 1,2-Dimethoxyethane (33 mL), THF (2.7 mL), and EHT (1.06 g) were added into the suspension of SiNP (1 g) in ethanol (5 mL) in a round bottom flask. The round bottomed flask was equipped with distillation apparatus and stirred at 95 °C. The solvent of about 27 mL was removed by azeotropic distillation.[56, 57] The concentrated suspension was stirred under refluxing at 80 °C for 15 h. The modified SiNP were washed by consecutive centrifugation (14000 rpm) and redispersion cycles in ethanol, acetone and toluene.

Finally, the suspension of the RAFT agent-fixed SiNP was solvent-exchanged to DMF by repeated redispersion/centrifugation to obtain a DMF stock suspension of the EHT-fixed SiNP.

The amount of EHT attached to the surface of the particles was determined by thermal gravimetry analysis (TGA). Equation (1) was used to calculate the grafting density (σ) of EHT on SiNP based on TGA results.[53, 58] Where, ρ is the density of silica nanoparticles (1.9×10^{-21} g·nm^{-3}), D is the average diameter of core particles (135 nm), $m_{(organic)}$ and $m_{(SiNP)}$ are the mass losses for EHT and silica nanoparticles, respectively acquired from TGA, N_A is the Avogadro's number and M_n is the molar mass of EHT.

$$\sigma = \frac{\rho D N_A m_{(organic)}}{6 M_n m_{(SiNP)}} \quad (1)$$

Self-initiated RAFT polymerization of styrene (S) on SiNP

Polymerization of styrene (S) with the RAFT-functionalised SiNP (with average diameter of 135 nm) was carried out as follows (Scheme 1): The RAFT agent (propionic acid)yl butyl trithiocarbonate (PABTC) was weighed into a round bottom flask, followed by addition of DMF (10 % of monomer mass). EHT-coated SiNP in DMF and styrene were then added to the mixture. The round bottom flask was equipped with a magnetic stirrer bar, sealed with a rubber septum and stirred for five minutes before taking sample for NMR analysis. The system was placed in an ice bath and deoxygenated by bubbling of nitrogen for 20 minutes. The polymerization was carried out in an oil bath (MR Hei-Standard, Heidolph Instruments) thermostated at 110 °C. After 18 hours a sample was taken out under nitrogen flow for NMR analysis. The polymerization was stopped after 23 hours by cooling the polymerization flask down to room temperature and exposing polymer to air. Small amounts of the solution were taken out for NMR analysis to determine monomer conversion. The rest of the reaction mixture was diluted by THF and centrifuged (14000 rpm) to collect polymer-grafted SiNP. The supernatant was used for SEC measurements to determine molar mass and its distribution of the free polymers. The cycles of centrifugation and redispersion in THF were repeated five times to obtain polymer-grafted SiNP perfectly free of the unbound (free) polymer. In a typical run, the polymerization of S was carried out at 110 °C with the starting

materials of S (5 g, 47.6 mmol), PABTC (2.8 mg, 11.9 μmol), EHT-fixed SiNP (55 mg), and DMF (0.56 g). This resulted in a monomer conversion of 41 % after 18 hours and 49 % after 23 hours producing a free polymer with M_n = 28700 g·mol^{-1} at the end of the polymerization and $Đ = M_w/M_n$ = 1.39, where M_n and M_w are the number- and weight-average molar masses, respectively.

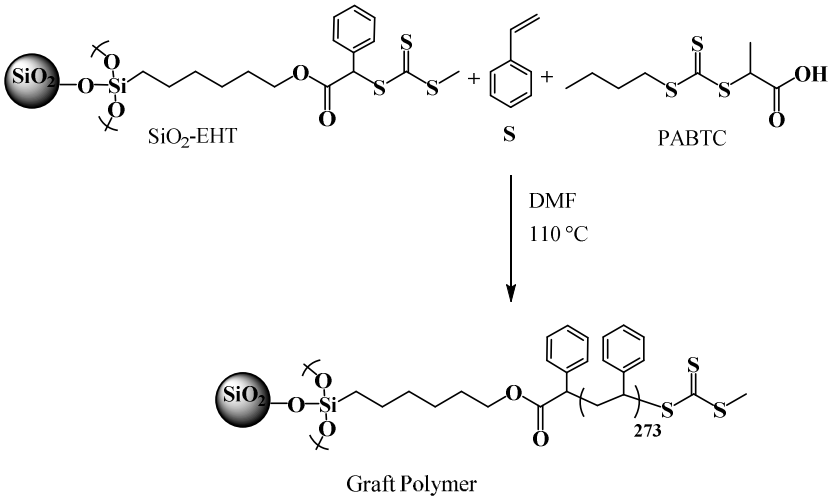

Scheme 1. Fabrication of silica-polystyrene hybrid particles by self-initiated RAFT polymerization. Free RAFT polymer from PABTC will be in the supernatant solution.

Cleaving of the PS chains from the silica nanoparticles

To determine the molar mass of the grafted polymer, PS brushes were cleaved from the surface of the SiNP as follows: the polymer-grafted SiNP (35 mg) were solvent exchanged with toluene (5 ml) via centrifugation and redispersion (2 cycles) and was transfer to a PE bottle. Subsequently the phase transfer agent Aliquat 336 (50 mg) was added followed by the addition of an aqueous solution of HF (25 %, 5 mL). The mixture was vigorously stirred for 3 h. The cleaved polymer in the organic layer was separated from HF phase and subjected to SEC measurements. M_n and M_w/M_n values of the grafted polymer were 28400 g.mol^{-1} and 1.21, respectively. To estimate the amount of the grafted polymer, hybrid particles (SiNP-PS) were subjected to thermogravimetric analysis.

RAFT polymerization of Styrene on SiNP with radical initiator

For this polymerization of styrene, 1,1'-azobis(cyclohexanecarbonitrile) (V40) was used as a source of radicals. In a typical run, prescribed amounts of free RAFT agent (PABTC), V40 (in different concentrations, (Table 2)) and DMF (10 % of monomer mass) were added to a round bottom flask equipped with a magnetic stirrer bar. To this mixture, SiNP in DMF and styrene were added (Table 2). The round bottom flask was sealed and the reagents were mixed thoroughly by stirring for around 5 minutes before deoxygenating by a flow of argon for 20 minutes in an ice bath. The polymerization was started by immersing the flask in an oil bath thermostated at 90 °C. NMR samples were taking out at the time zero, after 18 hours and also at the end of the polymerization to measure monomer conversion. The polymerization was stopped after 23 hours. Polystyrene-modified SiNP were purified from the free polymers and other unreacted reagents by 5 centrifugation and redispersion cycles in THF. The free polymer in supernatant solution was characterized by SEC. The amount of the grafted polymer was determined by thermogravimetric analysis (TGA). The hydrodynamic size of the hybrid particles was characterized by dynamic light scattering (DLS).

Self-assembly of hybrid particles as 3D colloidal crystals

(i) Self-assembly from suspension. For this self-assembly process, monodisperse and well-defined colloidal particles of SiNP-PS were dispersed in a mixed solvent with refractive index and density matching that of the particles.

(ii) Centrifugation. Highly uniform and well-defined colloidal particles of SiNP-PS were dispersed in isorefractive solvents and transferred into small polyethylene eppendorf tubes. The suspensions of these colloidal particles were spun at lower speed (5000 rpm) for 5 minutes and then for another 8 minutes at higher speed (13000 rpm).

Results and discussions

Preparation of polystyrene-grafted silica colloidal core-shell particles

Silica nanoparticles of two sizes, 135 nm and 75 nm, were used in this study. The smaller SiNP were prepared via the Stöber synthesis following the method described by Rao et al.[55] This fabrication route is particularly appropriate for the synthesis of small size silica nanoparticles, and led to a mean diameter determined by TEM of 75 nm (dry state) and 86 nm with a polydispersity index (*PDI*) of 0.08, as determined by DLS (solvated state), thus confirming a remarkably narrow size distribution when compared to commercial particles in this size range (see Figures S1a and S1b, Supporting Information).[59-61] Following attachment of the RAFT agent EHT to the SiNP, DLS measurements showed a slight increase in the hydrodynamic size of particles, due to the solvation of the surface-attached RAFT agent, whilst keeping narrow *PDI* (See Table 1). TGA analysis of the pale yellow particles before and after attachment showed that 2.32 % and 4.09 % of the EHT have been incorporated onto the 75 and 135 nm SiNP, respectively (Figure S2, Supporting Information). This corresponds to grafting densities of 0.97 and 2.40 trithiocarbonate groups/nm^2 for the 75 and 135 nm SiNP, respectively, with the assumption that all the mass loss from TGA arises from the attached RAFT agent.

Table 1. Dynamic light scattering measurements for bare SiNP and after modification with EHT.

	Before modification		After modification	
Samples	Diameter (nm)	*PDI*	Diameter (nm)	*PDI*
1	137	0.063	188	0.062
2	86	0.085	113	0.081

The EHT functionalised SiNP were subsequently used to perform surface-initiated RAFT polymerization of styrene (S). Polystyrene is an excellent candidate for the polymer shell of core-shell hybrid particles for its high refractive index contrast with the silica particles core.[53] Polymerizations were undertaken in the presence of a free RAFT agent (PABTC) in solution, in order to improve the control over the polymerization, as detailed in previous publications.[53, 54, 62] Indeed, PABTC not only contributes to the fast exchange of thiocarbonylthio group at the polymer chain ends, but also it prevents interparticle coupling and aggregation. Polymerizations were

undertaken in DMF (10 % of monomer mass) to obtain a good colloidal dispersibility during reaction.

In preliminary work, two alternative methods for the polymerization of styrene in the presence of the SiNP and PABTC were employed, by varying the initiation protocol, either by using a thermal radical initiator, 1,1'-azobis(cyclohexanecarbonitrile) (V40) at 90 °C, sample SiNP-PS2, or by self-initiation of the monomer at 110 °C, sample SiNP-PS1. Each reaction yielded an amount of SiNP set to 1 % of the monomer mass, in order to obtain good colloidal stability. The self-initiation polymerization was stopped at medium conversions, (48.7%, Figure S3, Supporting Information) to maintain good control. Previous works[48, 53, 62] has shown that the molar masses of free and grafted polymeric chains in RAFT polymerization are typically similar. We used the particles obtained from the self-initiated polymerization system to confirm this observation, by cleaving the polymer brushes from the SiNP by treatment with HF, revealing very close M_n values for free and grafted polymeric chains, 28,700 and 28,400 $g \cdot mol^{-1}$, respectively.

Polymerisations undertaken in the presence of the free radical azoinitiator V40 reached higher conversions and higher molar masses when compared to the self-initiation polymerizations (See conversions by ^1H NMR spectroscopy in Figure S4, Supporting Information), presumably due to a higher concentration in radicals arising from the higher rate of radicals generation when using an azonitiator. In addition, the polymerization proceeded to yield SiNP grafted with PS chains with a grafting density as high as 0.32 chains/nm^2.[53] The use of a free radical initiator was preferred as the method to prepare the core-shell particles, as it led to higher conversions. Table 2 summarises the characterisation of the various particles synthesised, and Figure 1 shows the SEC traces of the free polymers.

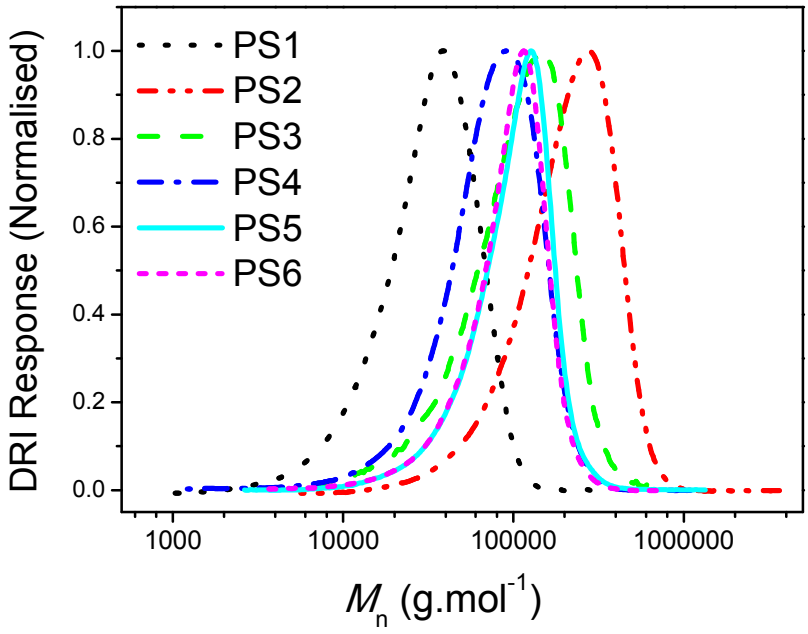

Figure 1. SEC traces for 6 different PS (free polymer) grown by self-initiation (PS1) and radical-initiation (PS2-PS6). Molar mass values (M_w) for PS1, PS2, PS3, PS4, PS5, PS6 are 38,300; 245,300; 124,000; 87,200; 108,200 and 105,600 g.mol^{-1}, respectively.

Table 2. Polymerization conditions and hydrodynamic sizes for the hybrid particles of SiNP-PS. The mass of DMF and SiNP-EHT were set to 10 % and 1 % of monomer mass, respectively. PABTC was used as a free RAFT agent in the solution. M_n and $Đ$ values are measured from the free polymers.

Samples	$[S]_0$ (mol/L)	$[PABTC]_0$ (mol/L)	$[V40]_0$ (mol/L)	SiNP-EHT [a] (mg)	Temperature (°C)	Conversion (%)	M_w (g/mol)	$Đ$	DLS Size[b] (nm)	*PDI* [d]	Grafting density, σ (chains/nm^2)	Compact core-shell diameter (nm)
SiNP-PS1	7.55	1.89E-03	-	55	110	49	38,300	1.39	257	0.06	0.19	150
SiNP-PS2	7.61	7.30E-04	8.40E-04	50	90	80	245,300	1.39	539	0.04	0.11	179
SiNP-PS3	7.57	3.60E-03	3.60E-03	55	90	83	124,000	1.40	457	0.05	0.21	178
SiNP [c]-PS4	6.11	2.88E-03	6.25E-03	50	90	80	87,200	1.52	390	0.07	0.32	112
SiNP-PS5	7.65	3.81E-03	3.76E-03	165	90	57	108,200	1.39	402	0.05	0.17	168
SiNP-PS6	7.87	5.24E-03	5.22E-03	300	90	91	105,600	1.22	352	0.01	0.16	169

[a] Pure SiNP-EHT are dispersed in DMF (18.3 %, w/w).

[b] DLS size based on the intensity measurements for hybrid particles.

[c] SiNP with a mean diameter of 75 nm. All the other hybrid particles have silica cores with diameter of 135 nm.

[d] From DLS measurements.

Dynamic light scattering measurements in dilute THF suspensions showed that the hydrodynamic diameter of the hybrid particles increases with increasing molar mass of the grafted polymers, to yield particles of diameter ranging 188 nm to 351 nm, whilst the polydispersity index (*PDI*) of SiNP-PS hybrid particles decreases, suggesting that the grafted polymer brushes cover SiNP uniformly. A thicker polymer shell around the SiNP was observed for the particles obtained by using a thermal free radical initiator, due to the high molecular weigh of the grafted polymers (Table 2 and Figure 2).

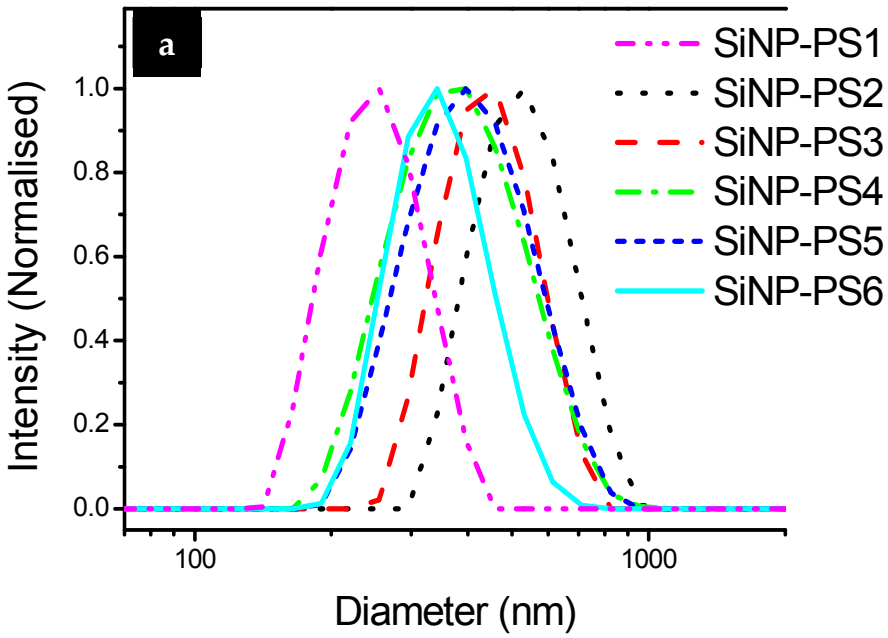

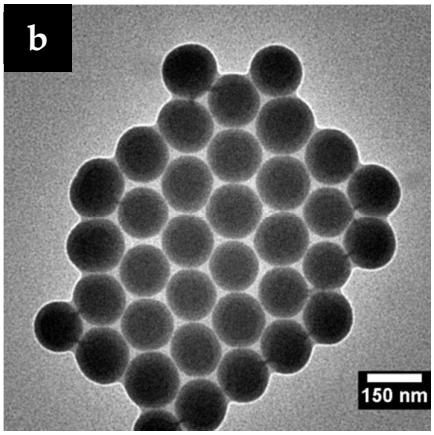

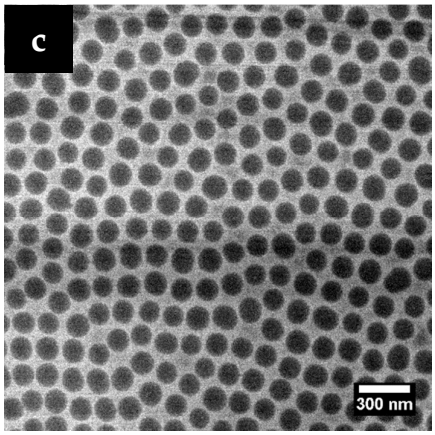

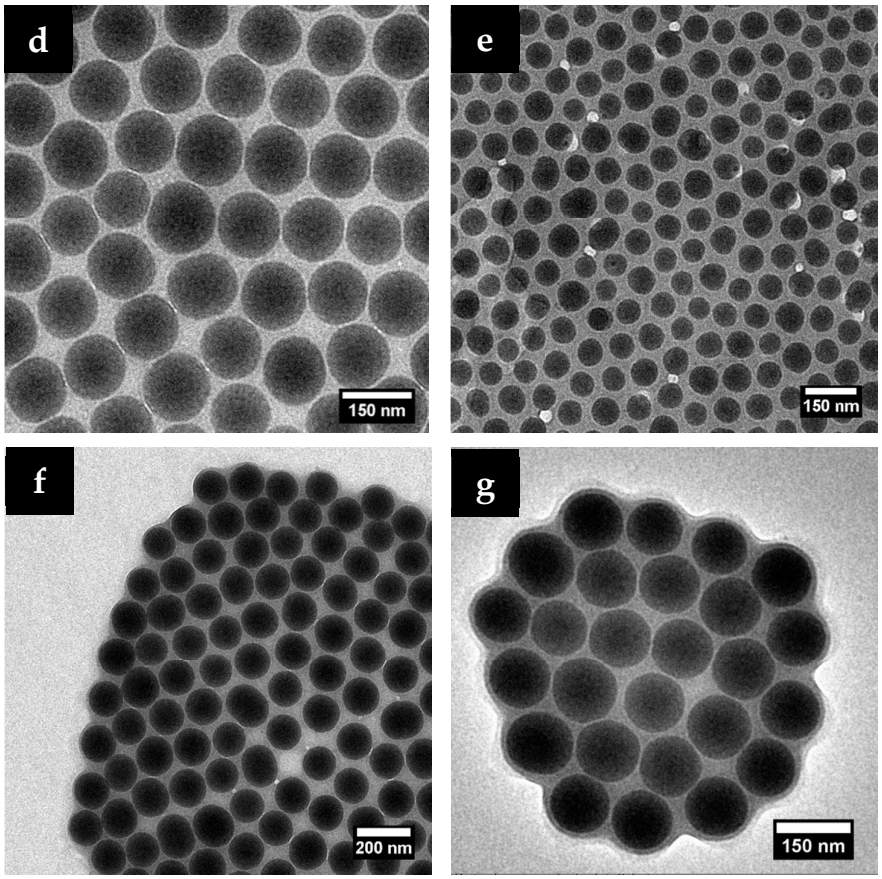

Figure 2. (a) DLS size distributions of 6 hybrid particles. (b), (c), (d), (e), (f) and (g) are TEM images of SiNP-PS1, SiNP-PS2, SiNP-PS3, SiNP-PS4, SiNP-PS5 and SiNP-PS6, respectively. The hydrodynamic size of hybrid particles are 257, 539, 457, 390, 402 and 352 nm for b, c, d, e, f and g, respectively.

The thickness of the polymer shell of the hybrid particles in their dry state was determined by the Compact Core-Shell model (Equation 2),[63, 64] where M_n is the number-average molar mass of polymer, σ is the grafting density of core-shell hybrid particles (calculated from equation (1)), N_A is Avogadro's number, d is the density of polymer, a is the radius of hybrid particles in dry state and r is the radius of silica core.

$$\frac{M_n \sigma 4\pi r^2}{N_A d_{polymer}} = \frac{4a^3\pi}{3} - \frac{4r^3\pi}{3} \qquad (2)$$

Table 2 summarises the grafting densities and the compact core-shell diameters (the diameter of the particles in their dry state, 2a) of all SiNP-PS hybrid particles. From this, we observe that the compact core-shell diameter matches relatively well the diameter observed by TEM (Figure 2). In addition, it is clear that the size of the hybrid particles in the dry state is both a function of molar mass and of the grafting density of the hybrid particles. Longer polymer brushes result in larger hybrid particles, and the compact diameter increases with the grafting density of the particles. This observation is in excellent agreement with other studies, for instance the work of Ebeling *et al.* who investigated the relationship between M_n of polymer brushes and interparticle spacing of core shell particles in the dry state, when grafting inorganic particles with polymeric chain anchored either through their chain-end or their side groups.[65]

Three-dimensional self-assembly and crystallization of polystyrene-grafted silica colloidal particles

The self-assembly and crystallisation of the colloidal SiNP-PS particles with hydrodynamic diameters ranging from 350 to 460 nm were investigated. In order to obtain nearly transparent suspensions, which is essential for the optical observations and also minimise the Van der Waals interactions between particles,[66-68] it is necessary to match the refractive index of solvent and particles. To find the effective refractive index (n_{eff}) of the hybrid particles, we performed thermogravimetric analysis. TGA results (Figure 3) showed mass losses of 40.5 %, 54 %, 32.9 % and 34.2 % for SiNP-PS3, SiNP-PS4, SiNP-PS5 and SiNP-PS6, respectively (For SiNP-PS1 see Figure S5, Supporting Information). These mass losses are in conformity with the grafting density of the polymer shell around the silica nanoparticles, the higher grafting density results in the larger mass loss in TGA.

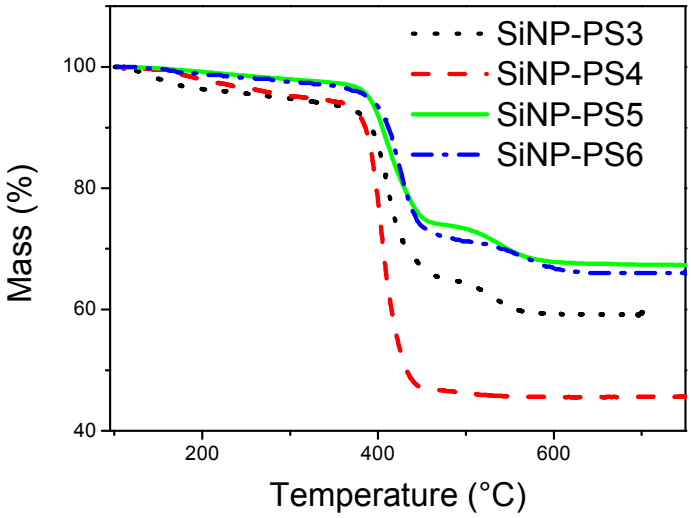

Figure 3. TGA analyses of four hybrid particles of SiNP-PS. Mass losses for SiNP-PS3, SiNP-PS4, SiNP-PS5 and SiNP-PS6 are 40.5 %, 54 %, 32.9 % and 34.2 %, respectively.

To calculate the effective refractive index (n_{eff}) of these hybrid particles we used Equation (3); where $\Phi_{polymer}$ and $n_{polymer}$ are weight fraction and refractive index of polystyrene, respectively and n_{SiNP} is the refractive index of silica nanoparticles. Considering the refractive indices of polystyrene and silica nanoparticles 1.59 and

1.45, respectively, the effective refractive indices for these hybrid particles were calculated at 1.51, 1.53, 1.50 and 1.50 for SiNP-PS3, SiNP-PS4, SiNP-PS5 and SiNP-PS6, respectively.

$$n_{eff} = \sqrt{\Phi_{polymer} \times n_{polymer}^{2} + (1 - \Phi_{polymer}) \times n_{SiNP}^{2}} \qquad (3)$$

Mixtures of chlorobenzene (Ph-Cl), *o*-dichlorobenzene (Ph-Cl_2) and 1,2-dichloroethane ($Cl_2C_2H_4$) with different volume ratios as solvent were used to match the refractive indices of hybrid particles (Table 3).

The colloidal particles were solvent exchanged from THF to the isorefractive mixed solvents. The typical procedure for the self-assembly and crystallization of colloidal particles is to let them equilibrate in an isobuoyant solvent by a suspension procedure. This procedure was demonstrated on similar systems by Ohno et al., who illustrated the remarkable properties of this type of core shell particles.[48, 53, 62] We adapted this methodology on our SiNP-PS6 hybrid particles (hydrodynamic diameter 352 nm; grafting density 0.16 chains·nm^{-2}; polystyrene shell of around M_n = 86000 g·mol^{-1} and $Đ$ = 1.22; refractive index 1.50; average density 1.61 g·cm^{-3}) to investigate their self-assembly. The hybrid particles were suspended in a nearly isobuoyant and isorefractive mixture of chloroform, *o*-dichlorobenzene and chlorobenzene with volume ratios of 52:46:2. The density matching reduces the effect of the gravity and provides an equilibrium state for the system. If the density of hybrid particles is much larger than that of the mixed solvent, particles will not be buoyant and tend to sediment, thus preventing the formation of micro crystals. On the other hand, matching the density of particles and medium results in negligible attraction forces and the repulsive forces dominate. The particles suspension of around 17.1 vol % was allowed to stand inside a sealed glass tube at ambient temperature. Clear iridescent flecks were observed within 6 hours of starting the self-assembly, indicating the formation of Bragg-reflecting crystallites inside the sample (Figure 4). The formed colloidal crystals (CC) were completely reproducible as they could self-assemble with the same iridescent flecks after they were agitated for three times.

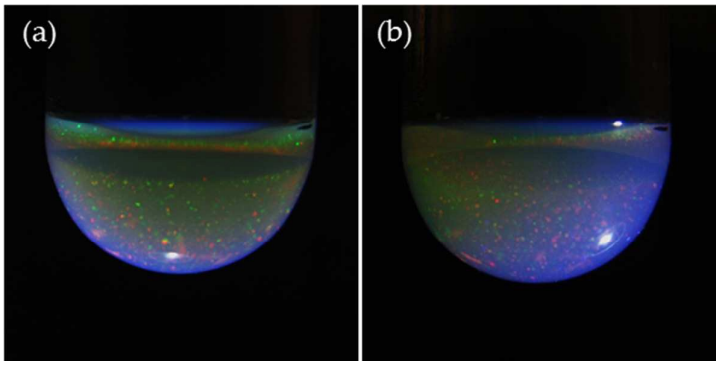

Figure 4. Digital photographs of microcrystals of SiNP-PS hybrid particles in the suspension of mixed solvents (chloroform, *o*-dichlorobenzene and chlorobenzene with volume ratios of 52:46:2) illuminated from bottom (a) and right side (b).

To investigate the crystal structure visually, the suspension of CC was transferred into a hand-made glass cell (Figure S6, Supporting Information), left to equilibrate for a few hours, and then subjected to confocal laser scanning microscope (CLSM) measurements. Figure 5 exhibits a CLSM image of a two-dimensional horizontal slice inside the sample in the reflective mode. The yellow dots represent silica core particles arranged in fcc stacking, surrounded by a polystyrene shell. The mean nearest-neighbour centre-to-centre distance (D_{ctc}) between the particles was found to be 355 nm, which correlate well with the hydrodynamic diameter determined by DLS. The distance can also be estimated from the volume fraction, φ, of the particles in crystal, according to the Equation (4), which is valid for close-packed structures.[46]

$$D_{theo} = 2^{1/6}\left(V_p / \varphi\right)^{1/3} \qquad (4)$$

Where V_p is a volume of a SiNP-PS particle in the unit of nm^3. D_{theo} value was calculated to be 290 nm, which is in reasonable agreement with the experimentally observed D_{ctc}.

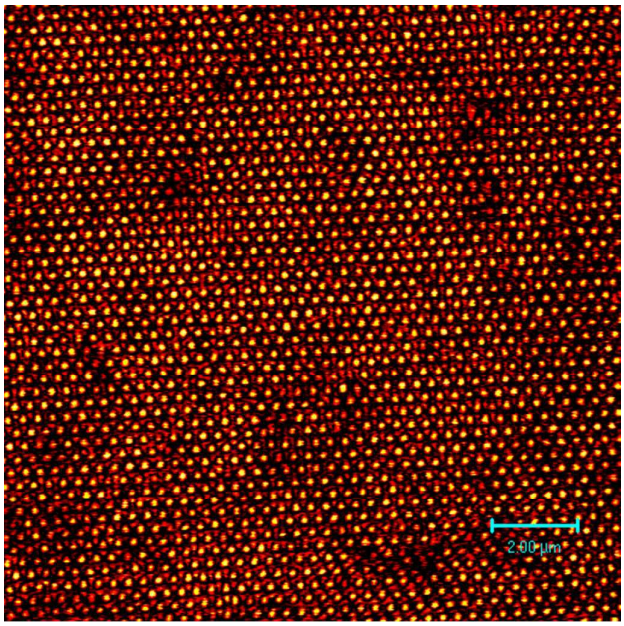

Figure 5. Confocal laser scanning microscopic (CLSM) image of colloidal crystal of SiNP-PS6 hybrid particles. Observation was performed using an Ar laser of wavelength 488 nm and x63 objective in reflection mode. Yellow dots represent silica core particles surrounded by dark polystyrene shells. The scale bar is 2 µm.

Having demonstrated the ability of our particles to assemble into colloidal crystals, we were interested in exploring a more versatile approach to obtain the crystals. We anticipated that the uniformity of our particles and their ability to self-correct their assembly, due to the 'soft' interparticle interactions arising from the steric repulsion of the polymer shell, might permit to simply use centrifugation of the particle in solution to form the colloidal crystals. This approach is far less demanding than the sedimentation procedure, in terms of time and technical set up. The only consideration for this approach is to ensure that the density of the solvent in which the particles are dispersed is lower than the density of the hybrid. Therefore, a series of mixed solvent were designed with appropriate densities, see Table 3.

Table 3. Effective refractive indices of four different SiNP-PS based on TGA analyses. Mixed solvents of chlorobenzene (Ph-Cl), *o*-dichlorobenzene (Ph-Cl_2) and 1,2-dichloroethane ($Cl_2C_2H_4$) with different volume ratios were used to match the refractive indices of the hybrid particles.

Sample	Mass loss (%)	n_{eff}	Solvent mixture	Solvent ratio (v/v)
SiNP-PS3	40.5	1.51	Ph-Cl/$Cl_2C_2H_4$	70/30
SiNP-PS4 [a]	54.0	1.53	Ph-Cl/Ph-Cl_2	50/50
SiNP-PS5	32.9	1.50	Ph-Cl/$Cl_2C_2H_4$	55/45
SiNP-PS6	34.2	1.50	Ph-Cl_2/$Cl_2C_2H_4$	50/50

[a] size of the silica cores is 75 nm. For all the other hybrid particles the size of silica cores was 135 nm.

The hybrid particles were centrifuged in their corresponding mixed solvents at 6000 rpm for 5 minutes, followed by an increased spinning rate to 14000 rpm for another 8 minutes. The spinning rate is an important factor and is related to the particles size and density. Spinning is typically started at a low rate to give enough time to the colloidal particles to arrange themselves into ordered arrays. Increasing the spinning rate forces the particles to pack themselves closely in well organised 3D structures. After formation of the colloidal crystals in the bottom of the eppendorf tube, a clear iridescent reflection was observed upon illumination by white light. As shown in Figure 6 (from a to i), the iridescent color of these colloidal crystals change as the angle of incident light varies which indicates the existence of a stop band according to Bragg's Law.[69, 70]

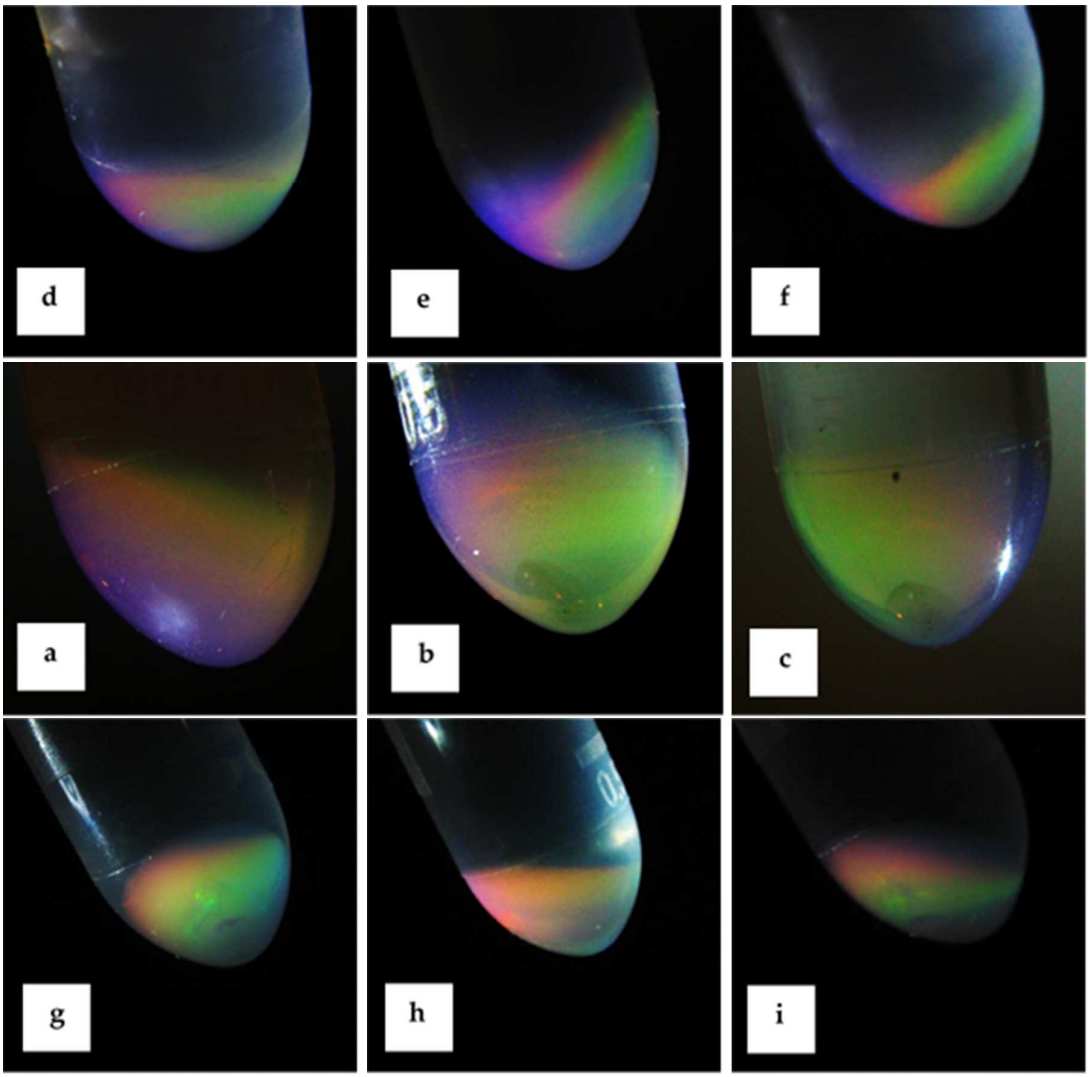

Figure 6. Photographs of colloidal crystals after illuminating samples with white light from different angles: (a), (b) and (c) from SiNP-PS3 in chlorobenzene / 1,2-dicloroethane (70/30:v/v); (d), (e) and (f) from SiNP-PS5 in chlorobenzene / *o*-dichlorobenzene (50/50:v/v); (g), (h) and (i) from SiNP-PS6 *o*-dichlorobenzene / 1,2-dichloroethane (50/50:v/v).

We were not able to run UV–Vis spectroscopy of the colloidal crystals (CC) in the eppendorf tube. Instead, a small quantity of the SiNP-PS3 hybrid particles were centrifuged in a thin cuvette at lower speed for a longer time. Transmission spectrum confirmed the existence of a Bragg peak at 556 nm (Figure 7). The position of the Bragg peak (556 nm) corresponds to a lattice constant of 184 nm calculated from Bragg's Equation (Equation 5) for the close-packed face-centred cubic (fcc) lattice.

$$\lambda = 2d(n_{eff}^2 - \sin^2\theta)^{1/2} \quad (5)$$

Where λ, is the position of Bragg peak in transmission spectrum, n_{eff} is the effective refractive index of colloidal particle, d is the lattice constant and θ is the angle of the incident light to crystal plane. Note that the effective refractive index of these hybrid particles is 1.51 and the incident light is normal (θ = 180 °).

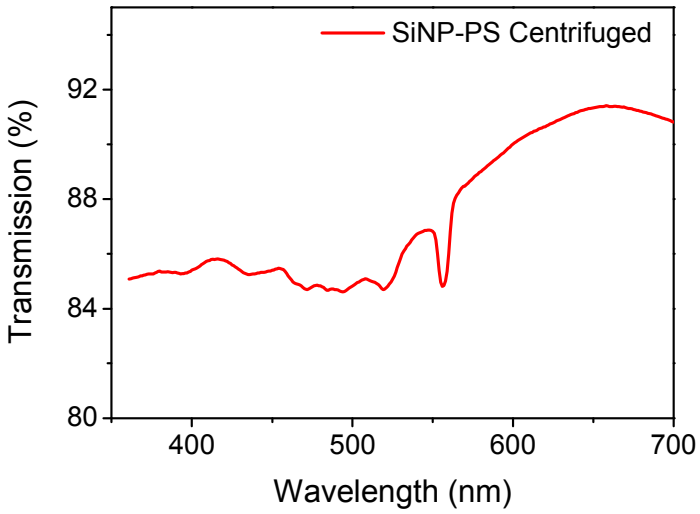

Figure 7. Transmission spectra of colloidal crystals in a quartz cuvette acquired by Cary 5000 spectrophotometer.

The angle-dependant iridescent color visually observed when changing viewing angle for these colloidal crystals is also a strong sign of the existence of a stop band, as demonstrated by Kitamura's group.[71] The assembly of colloidal spheres by centrifugation results in the formation of colloidal crystals with two spontaneous orientation of (100) and (111) as shown by Jensen el at.[72] (110) orientation is a significantly less dense crystal plane and never appears as a spontaneously occurring texture on a flat surface. Some extended defects such as dislocations and stacking faults are also present in the formed colloidal crystals. As the thickness of colloidal crystals exceeds the critical thickness, a significant concentration of theses stacking faults is acquired which results in destruction of stop band and consequently iridescent colors.

For the sample SiNP-PS4, no iridescent reflection was observed which indicates the absence of crystalline planes. A possible reason for this observation is the lack of

uniformity of the small size 75 nm SiNP employed (Figure 2e). This revealed that regardless of the high grafting density of polymer shell around these particles, formation of colloidal crystals requires very well-defined core particles and the presence of a thick polymer shell cannot compensate uniformity of core particles when they undergo strong centrifugational forces.

Conclusion

Monodisperse silica nanoparticles (SiNP) with an average diameters of 75 and 135 nm were functionalized with a chain transfer agent (EHT) and subsequently used for RAFT-mediated graft polymerization of styrene. The fabricated core-shell hybrid particles (SiNP-PS) were uniform and well-defined with high grafting density as 0.3 chains·nm^{-2}, which made them potential candidates for self-assembly and crystallization. Adjusting the refractive indices and the density of the hybrid particles with those of mixed solvents enabled the formation of iridescent and buoyant microcrystals by self-assembly of the particles throughout the entire suspension. We also showed that the narrow size distribution of the particles enabled the formation of 3D colloidal crystals with variable reflected colours by simple centrifugation of the colloidal solution, an approach much more versatile, simpler and faster than the traditional sedimentation technique.

Acknowledgements

The authors thank the Australian Centre for Microscopy and Microanalysis for electron microscopy and A/Prof Brian Hawkett for useful discussions. This work was supported in part by a grant from the Surface Coatings Association Australia (HS). The Australian Government is acknowledged for an Australian Postgraduate Award (HS), the Royal Society Wolfson Merit Award (WM130055; SP), the Monash-Warwick Alliance (SP) are also acknowledged for financial support.

References

1. E. Yablonovitch, *Phys. Rev. Lett.*, 1987, **58**, 2059-2062.
2. S. John, *Phys. Rev. Lett.*, 1987, **58**, 2486-2489.

3. C. López, *J. Opt. A: Pure Appl. Opt.*, 2006, **8**, R1.
4. A. Arsenault, S. Fournier-Bidoz, B. Hatton, H. Miguez, N. Tetreault, E. Vekris, S. Wong, S. Ming Yang, V. Kitaev and G. A. Ozin, *J. Mater. Chem.*, 2004, **14**, 781-794.
5. M. Calcerrada, P. Roy, C. García-Ruiz and M. González-Herráez, *Sens. Actuators: B Chem.*, 2014, **191**, 264-269.
6. R. De Angelis, I. Venditti, I. Fratoddi, F. De Matteis, P. Prosposito, I. Cacciotti, L. D'Amico, F. Nanni, A. Yadav, M. Casalboni and M. V. Russo, *J. Colloid Interface Sci.*, 2014, **414**, 24-32.
7. P. N. Pusey and W. Vanmegen, *Nature*, 1986, **320**, 340-342.
8. A. Yethiraj and A. van Blaaderen, *Nature*, 2003, **421**, 513-517.
9. O. Azzaroni, *J. Polym. Sci., Part A: Polym. Chem.*, 2012, **50**, 3225-3258.
10. R. Patel, W. S. Chi, S. H. Ahn, C. H. Park, H.-K. Lee and J. H. Kim, *Chem. Eng. J.*, 2014, **247**, 1-8.
11. H. Takano, B. S. Song, T. Asano, S. Noda and Ite, *J. Inst. Image Info. Television Engi.*, 2005, **1&2**, 1989-1992.
12. H. Takano, B.-S. Song, T. Asano and S. Noda, *Appl. Phys. Lett.*, 2005, **86**, 241101-241103.
13. T. A. Taton and D. J. Norris, *Nature*, 2002, **416**, 685-686.
14. H. Xu, K.-D. Cao, H.-B. Ding, Q.-F. Zhong, H.-C. Gu, Z.-Y. Xie, Y.-J. Zhao and Z.-Z. Gu, *ACS Appl. Mater. Interface*, 2012, **4**, 6752-6757.
15. S. Perrier and P. Takolpuckdee, *J. Polym. Sci., Part A: Polym. Chem.*, 2005, **43**, 5347-5393.
16. S. Furumi, H. Fudouzi, H. T. Miyazaki and Y. Sakka, *Adv. Mater.*, 2007, **19**, 2067-2072.
17. S. Février, D. D. Gaponov, P. Roy, M. E. Likhachev, S. L. Semjonov, M. M. Bubnov, E. M. Dianov, M. Y. Yashkov, V. F. Khopin, M. Y. Salganskii and A. N. Guryanov, *Opt. Lett.*, 2008, **33**, 989-991.
18. J. R. Lawrence, Y. Ying, P. Jiang and S. H. Foulger, *Adv. Mater.*, 2006, **18**, 300-303.
19. H. Yamada, T. Nakamura, Y. Yamada and K. Yano, *Adv. Mater.*, 2009, **21**, 4134-4138.
20. D. Aurélien, B. Henri and W. Claude, *Rep. Prog. Phys.*, 2012, **75**, 126501.
21. T.-S. Deng, J.-Y. Zhang, K.-T. Zhu, Q.-F. Zhang and J.-L. Wu, *Mater. Chem. Phys.*, 2011, **129**, 540-546.
22. F. Gallego-Gómez, A. Blanco, V. Canalejas-Tejero and C. López, *Small*, 2011, **7**, 1838-1845.
23. Y. Li, F. Piret, T. Leonard and B. L. Su, *J. Colloid Interface Sci.*, 2010, **348**, 43-48.
24. S. Schutzmann, I. Venditti, P. Prosposito, M. Casalboni and M. V. Russo, *Opt. Express*, 2008, **16**, 897-907.
25. E. Yablonovitch, *J. Phys.*, 1987, **48**, 615-616.
26. J. Zhu, M. Li, R. Rogers, W. Meyer, R. H. Ottewill, S. T. S. S. S. Crew, W. B. Russel and P. M. Chaikin, *Nature*, 1997, **387**, 883-885.
27. T. Okubo, *Prog. Polym. Sci.*, 1993, **18**, 481-517.
28. K. Ohno, *Polym. Chem.*, 2010, **1**, 1545-1551.
29. P. Jiang, J. F. Bertone, K. S. Hwang and V. L. Colvin, *Chem. Mater.*, 1999, **11**, 2132-2140.
30. X. Zhang, J. Zhang, D. Zhu, X. Li, X. Zhang, T. Wang and B. Yang, *Langmuir*, 2010, **26**, 17936-17942.

31. R. C. Hayward, D. A. Saville and I. A. Aksay, *Nature*, 2000, **404**, 56-59.
32. Y. H. Kim, J. Park, P. J. Yoo and P. T. Hammond, *Adv. Mater.*, 2007, **19**, 4426-4430.
33. K. Ohno, T. Morinaga, S. Takeno, Y. Tsujii and T. Fukuda, *Macromolecules*, 2007, **40**, 9143-9150.
34. K. Ohno, T. Morinaga, S. Takeno, Y. Tsujii and T. Fukuda, *Macromolecules*, 2006, **39**, 1245-1249.
35. A. Stein, B. E. Wilson and S. G. Rudisill, *Chem. Soc. Rev.*, 2013, **42**, 2763-2803.
36. W. Sun, F. Jia, Z. Q. Sun, J. H. Zhang, Y. Li, X. Zhang and B. Yang, *Langmuir*, 2011, **27**, 8018-8026.
37. Y. Xu, G. K. German, A. F. Mertz and E. R. Dufresne, *Soft Matter*, 2013, **9**, 3735-3740.
38. Q. Yan, L. K. Teh, Q. Shao, C. C. Wong and Y.-M. Chiang, *Langmuir*, 2008, **24**, 1796-1800.
39. J. Hilhorst, D. A. M. de Winter, J. R. Wolters, J. A. Post and A. V. Petukhov, *Langmuir*, 2013, **29**, 10011-10018.
40. J. P. Hoogenboom, D. Derks, P. Vergeer and A. van Blaaderen, *J. Chem. Phys*, 2002, **117**, 11320-11328.
41. Y. K. Koh, L. K. Teh and C. C. Wong, *Thin Solid Films*, 2008, **516**, 5637-5639.
42. Z.-Y. Li and Z.-Q. Zhang, *Phys. Rev. B: Condens. Matter*, 2000, **62**, 1516-1519.
43. K.-h. Lin, J. C. Crocker, V. Prasad, A. Schofield, D. A. Weitz, T. C. Lubensky and A. G. Yodh, *Phys. Rev. Lett.*, 2000, **85**, 1770-1773.
44. Y. A. Vlasov, V. N. Astratov, A. V. Baryshev, A. A. Kaplyanskii, O. Z. Karimov and M. F. Limonov, *Phys. Rev. E: Stat. Phys., Plasmas, Fluids,*, 2000, **61**, 5784-5793.
45. K. Ohno, T. Morinaga, K. Koh, Y. Tsujii and T. Fukuda, *Macromolecules*, 2005, **38**, 2137-2142.
46. T. Morinaga, K. Ohno, Y. Tsujii and T. Fukuda, *Macromolecules*, 2008, **41**, 3620-3626.
47. Y. Huang, T. Morinaga, Y. Tai, Y. Tsujii and K. Ohno, *Langmuir*, 2014, **30**, 7304-7312.
48. J. Moraes, K. Ohno, T. Maschmeyer and S. Perrier, *Chem. Commun.*, 2013, **49**, 9077-9088.
49. J. Moraes, K. Ohno, G. Gody, T. Maschmeyer and S. Perrier, *Beilstein J. Org. Chem.*, 2013, **9**.
50. J. Moraes, K. Ohno, T. Maschmeyer and S. Perrier, *Chem. Mater.*, 2013, **25**, 3522-3527.
51. X. Ye and L. Qi, *Sci. China Chem.*, 2014, **57**, 58-69.
52. G. Moad, E. Rizzardo and S. H. Thang, *Aust. J. Chem.*, 2012, **65**, 985-1076.
53. K. Ohno, Y. Ma, Y. Huang, C. Mori, Y. Yahata, Y. Tsujii, T. Maschmeyer, J. Moraes and S. Perrier, *Macromolecules*, 2011, **44**, 8944-8953.
54. H. Sabouri, K. Ohno and S. Perrier, *Polym. Chem.*, 2015, DOI: 10.1039/C5PY00912J
55. K. S. Rao, K. El-Hami, T. Kodaki, K. Matsushige and K. Makino, *J. Colloid Interface Sci.*, 2005, **289**, 125-131.
56. J.-S. Im, J.-H. Lee, S.-K. An, K.-W. Song, N.-J. Jo, J.-O. Lee and K. Yoshinaga, *J. Appl. Polym. Sci.*, 2006, **100**, 2053-2061.
57. K. Yoshinaga and Y. Hidaka, *Polym. J.*, 1994, **26**, 1070-1079.
58. M. Zhang, L. Liu, C. Wu, G. Fu, H. Zhao and B. He, *Polymer*, 2007, **48**, 1989-1997.

59. A. Beganskienė, V. Sirutkaitis, M. Kurtinaitienė, R. Juškėnas and A. Kareiva, *Mater. Sci. Medzg.*, 2004, **10**, 287-290.
60. I. A. Ibrahim, A. Zikry and M. A. Sharaf, *J American Sci*, 2010, **6**, 985-989.
61. I. A. M. Ibrahim, A. A. F. Zikry, M. A. Sharaf, J. E. Mark, K. Jacob, I. M. Jasiuk and R. Tannenbaumn, *IOP Conference Series: Mater. Sci. Engi.*, 2012, **40**, 012008.
62. Y. Tsujii, M. Ejaz, K. Sato, A. Goto and T. Fukuda, *Macromolecules*, 2001, **34**, 8872-8878.
63. K. Ohno, K. Koh, Y. Tsujii and T. Fukuda, *Angew. Chem. Int. Ed.*, 2003, **42**, 2751-2754.
64. T. Morinaga, K. Ohno, Y. Tsujii and T. Fukuda, *Eur. Polym. J.*, 2007, **43**, 243-248.
65 B. Ebeling, P. Vana, *Macromolecules* 2013, **46**, 4862−4871
66. A. Brands, H. Versmold and W. van Megen, *J. Chem. Phys*, 1999, **110**, 1283-1289.
67. S.-H. Kim, S.-H. Kim, W. C. Jeong and S.-M. Yang, *Chem. Mater.*, 2009, **21**, 4993-4999.
68. R. S. Pillai, M. Oh-e, H. Yokoyama, G. J. Brakenhoff and M. Müller, *Opt. Express*, 2006, **14**, 12976-12983.
69. C. I. Aguirre, E. Reguera and A. Stein, *Adv. Funct. Mater.*, 2010, **20**, 2565-2578.
70. C. Zhou, J. Han and R. Guo, *J. Colloid Interface Sci.*, 2013, **397**, 80-87.
71. T. Kanai, T. Sawada, J. Yamanaka and K. Kitamura, *J. Am. Chem. Soc.*, 2004, **126**, 13210-13211.
72. K. E. Jensen, D. Pennachio, D. Recht, D. A. Weitz and F. Spaepen, *Soft Matter*, 2013, **9**, 320-328.